NDT&E International 66 (2014) 82–89

Contents lists available at ScienceDirect

NDT&E International

journal homepage: www.elsevier.com/locate/ndteint

Near electrical resonance signal enhancement (NERSE) in eddy-current crack detection

R. Hughes [a,*], Y. Fan [a], S. Dixon [a,b]

[a] Department of Physics, University of Warwick, Gibbet Hill Road, Coventry, CV4 7AL, United Kingdom
[b] School of Engineering, University of Warwick, Gibbet Hill Road, Coventry, CV4 7AL, United Kingdom

ARTICLE INFO

Article history:
Received 5 September 2013
Received in revised form
23 April 2014
Accepted 30 April 2014
Available online 9 May 2014

Keywords:
Eddy-current
Electrical Resonance
Electromagnetic
NDT
NDE
Crack Detection

ABSTRACT

An investigation was performed into the effects of operating an absolute eddy-current testing (ECT) probe at frequencies close to its electrical resonance. A previously undocumented defect signal enhancement phenomenon, resulting from associated shifts in electrical resonant frequency, was observed and characterized. Experimental validation was performed on three notch defects on a typical aerospace superalloy, Titanium 6Al–4V. A conventional absolute ECT probe was operated by sweeping through a frequency range about the electrical resonance of the system (1 – 5 MHz). The phenomenon results in signal-to-noise ratio (SNR) peak enhancements by a factor of up to 3.7, at frequencies approaching resonance, compared to those measured at 1 MHz. The defect signal enhancement peaks are shown to be a result of resonant frequency shifts of the system due to the presence of defects within the material. A simple, operational approach for raising the sensitivity of conventional industrial eddy-current testing is proposed, based on the principles of the observed near electrical resonance signal enhancement (NERSE) phenomenon. The simple procedural change of operating within the NERSE frequency band does not require complex probe design, data analysis or, necessarily, identical coils. Therefore, it is a valuable technique for improving sensitivity, which complements other ECT methods.

1. Introduction

Eddy-current testing (ECT) is a well-established non-destructive testing (NDT) technique, routinely implemented in industry for the inspection of safety-critical metallic components, because of its high sensitivity to small surface defects.

High-strength, low density superalloys are used frequently for many industrial applications, particularly in Aerospace [1]. The design and service lifetime of components is based on the assumption that the smallest defect that can be reliably detected by NDT techniques is present in the part. For this reason, research is generally focused on detecting smaller defects. Industrial eddy-current methods can reliably detect 0.75 mm long (max 0.38 mm deep) surface-breaking cracks, but achieving greater sensitivity is hampered by poor signal-to-noise ratios (SNR) [2]. Conventional ECT inspections operate in a range between 100 Hz and 1 MHz [3], so as to avoid the detrimental effects of environmental noise and the instabilities of electrical resonance. However, superalloys typically have very low electrical conductivities, leading to relatively large electromagnetic skin-depths at these frequencies. As a result, conventional operation does not provide sufficient resolution to the smallest defects, for which higher frequencies must be used.

Higher frequency inspections are not without their problems. They suffer from a greater susceptibility to liftoff, and variable surface conditions due to machining features or conductivity changes associated with shot-peening or burnishing (common in many manufacturing processes) [4,5]. This can lead to higher levels of background noise.

An effective approach for maximizing the SNR of any ECT defect inspection is to use signal averaging, but in an industrial environment this is not always possible or practical, where time and throughput are important financial considerations. Averaging will also have a negligible SNR improvement on materials that have random but coherent noise (i.e. grain structure). Whilst eddy-current arrays (ECAs) are becoming more commonplace in industrial use [6–8] because of their ability to inspect large areas very quickly, these advantages often come at the cost of resolution and sensitivity. Therefore, it is desirable to develop and implement techniques that can maximize the sensitivity of single coil and arrayed eddy current probes.

Many authors have implemented multi-frequency, data fusion techniques [9–11] to cancel out unwanted signals, such as liftoff and temperature variations, so as to improve the SNR. Although techniques such as these have had success in laboratory environments, their application in industry is limited by the longer

* Corresponding author. Tel.: +44 2476151778.
E-mail address: Robert.Hughes@warwick.ac.uk (R. Hughes).

http://dx.doi.org/10.1016/j.ndteint.2014.04.009

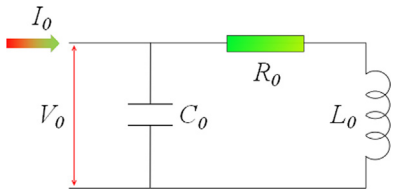

Fig. 1. Equivalence circuit in air. Simplified electronic circuit for an eddy-current probe in free space with a capacitive coaxial cable connection.

inspection times, complex operation and sophisticated signal processing algorithms [2,12,13] required. As a result such techniques are not commonly used in ECAs.

Authors such as Owston [14], Liu [15,16] and Ko [17,18] have recognized the potential of measuring the shifting of electrical resonant frequency, due to changes in its environment, as a highly sensitive means of measuring proximity, surface roughness and surface conductivity variations. The significant power transfer and large rates of change around high quality factor resonance peaks in the electrical impedance of an eddy current coil and cable, offer an extended dynamic range of impedance measurements. Such advantages make operating at frequencies around resonance highly sensitive to even the slightest changes in an electromagnetically coupled system, but currently there is no documented account of authors exploiting resonance effects specifically for defect detection.

An investigation was performed on the effects of operating an absolute ECT probe at frequencies approaching and passing electrical resonance. The research presented in this paper documents the initial findings of the investigation and highlights the implications that the work will have on future defect inspection techniques.

2. Theory

2.1. Electrical resonance

An eddy-current sensor is an electromagnetic inductor coil, connected to a current source via a coaxial cable. It can be very simply modeled as a parallel inductor–capacitor (LC) circuit with additional series resistive components [19] as shown in Fig. 1. The inductive component represents the coil and the capacitive component represents the coaxial cable. Contributions to the capacitance from adjacent coil turns are considered negligible, compared to the dominant capacitive interactions within the coaxial cable.

For the case of high frequencies, the resistive component can be considered negligible compared to the inductive reactance component ($R_0 \ll \omega L_0$). As a result the total impedance of the system is equivalent to the impedance between a parallel capacitor and an inductor. An expression can be obtained for Z_0 by the summation of component admittance ($Y = 1/Z$) and taking the reciprocal, such that [20],

$$Z_0 = \frac{R_0 + j\omega L_0}{1 + j\omega R_0 C_0 - \omega^2 L_0 C_0}. \quad (1)$$

Consequently, there will be a frequency at which the denominator of Eq. (1) becomes zero, and thus the impedance tends towards a maximum (Fig. 2). The system is in a state of parallel LC electrical resonance at the resonant frequency, $\omega_0 = 2\pi f_0$.

$$\omega_0 = \sqrt{\frac{1}{L_0 C_0}}. \quad (2)$$

The impedance to the flow of current is a maximum at resonance, and thus the voltage across the coil required to drive the same current through the system must increase to a maximum. As the system goes through its primary resonance, the phase will change from a positive (predominantly inductive) regime, to a negative (predominantly capacitive) regime (Fig. 2). Beyond resonance, the reactance is dominated by the capacitive effects in the coil [21], and the probe will cease to measure changes in the inductive component efficiently. Complex systems have multiple resonances occurring at higher frequencies as the electrical significance of the components resonating decreases.

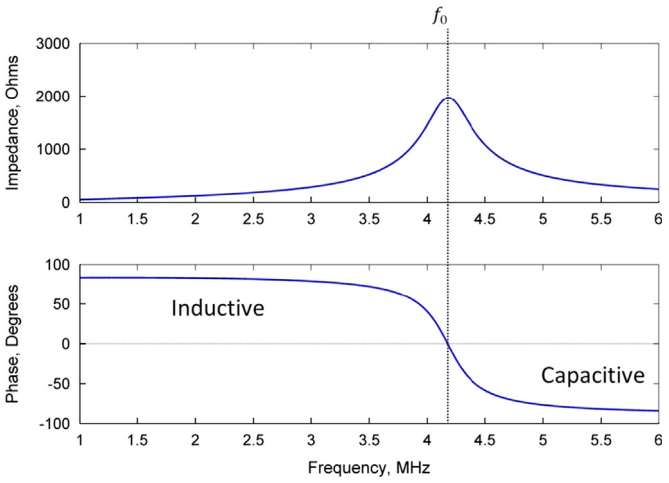

Fig. 2. Electrical resonance in air. The magnitude and phase of impedance of an ECT coil as it passes through the resonant frequency, f_0.

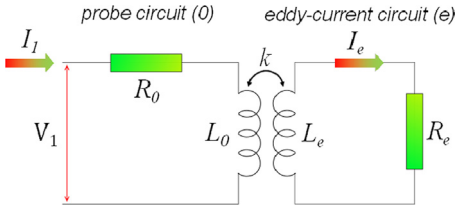

Fig. 3. Mutual inductance transformer model. Simple transformer circuit model for an eddy-current probe (0) coupled to the surface of an electrically conducting material (e).

This model represents an ECT coil in air but when brought into the proximity of an electrically conducting material, electromagnetic coupling occurs between the coil and the material surface. The equivalence circuit can be extended to model the coupling interaction, and has been utilized by many authors [14,16,22].

2.2. Mutual induction model

When an inductor is brought into proximity of an electrically conducting material, it will electromagnetically couple to the eddy-currents generated in the material surface. Coupling to the surface of a material changes the electrical properties of the probe such that the system can be approximated to an equivalent circuit containing components whose values change with the amount of coupling. The coupling interaction can be modeled by the transformer circuit diagram shown in Fig. 3 where the eddy-currents are modeled are a passive series inductor and resistance (LR) circuit [14].

The impedance of the inductive arm of the system, $Z_{1,L}$, can be formulated using Kirchoff's laws [23].

$$Z_{1,L} = R_0 + j\omega L_0(1-k^2) + \frac{\omega L_0 R_e k^2}{R_e^2 + \omega^2 L_e^2}(\omega L_e + jR_e). \quad (3)$$

By approximating uniform magnetic field interactions, the resistive and inductive-reactance components of the secondary

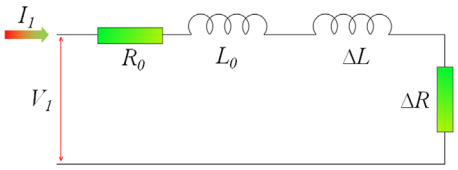

Fig. 4. Coupled ECT system equivalence circuit, adapted from Wheeler [22].

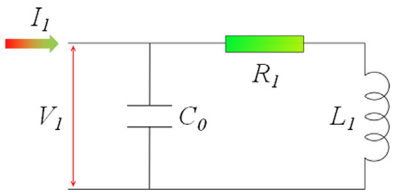

Fig. 5. Coupled eddy-current probe equivalence circuit with effective resistance and inductance.

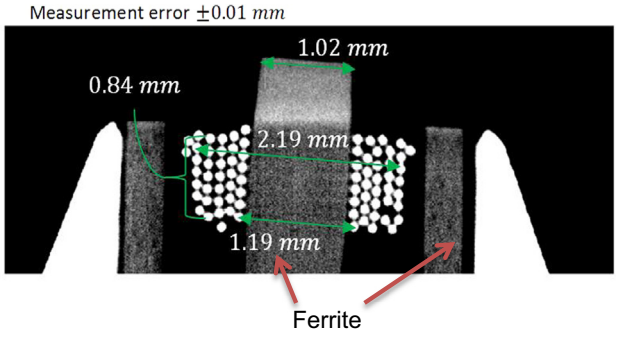

Fig. 6. Eddy-current probe. X-Ray CT cross-sectional image of pen probe coil with ferrite core and shielding cap. Credit: Rolls-Royce NDE lab, Bristol, UK.

circuit are assumed to be equal in magnitude ($\omega L_e = R_e$) as shown by Wheeler [22]. The impedance of the inductive arm of the circuit, $Z_{1,L}$, of the circuit in Fig. 3 therefore reduces to the series combination of the probe coil impedance in air, $Z_{0,L}$, plus additional series resistance and reactance of equal magnitude and frequency dependence.

$$Z_{1,L} = R_0 + j\omega L_0 + \frac{1}{2}\omega L_0 k^2 (1-j), \tag{4}$$

$$Z_{1,L} = Z_{0,L} + \frac{1}{2}\omega L_0 k^2 (1-j). \tag{5}$$

The result is consistent with the equivalence circuit proposed by Wheeler [22] for a uniform excitation field as shown in Fig. 4.

As a result the circuit diagrams in Figs. 3 and 4 can be remodeled as a single equivalence inductive circuit with effective inductive (L_1) and resistive (R_1) components (Fig. 5).

$$Z_{1,L} = R_1 + j\omega L_1, \tag{6}$$

$$R_1 = R_0 + \Delta R = R_0 + \frac{1}{2}\omega L_0 k^2, \tag{7}$$

$$L_1 = L_0 + \Delta L = L_0\left(1 - \frac{1}{2}k^2\right). \tag{8}$$

In the same way as the free space case in Section 2.1, the total impedance of the system is given by,

$$Z_1 = \frac{R_1 + j\omega L_1}{1 + j\omega C_0 R_1 - \omega^2 C_0 L_1}. \tag{9}$$

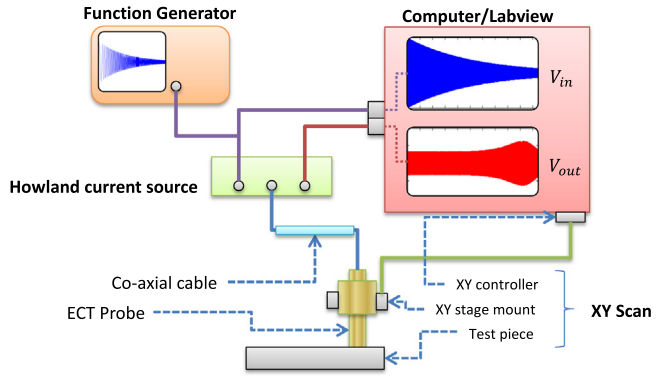

Fig. 7. Experimental set-up. Schematic diagram of the experimental set up for a 2D, frequency sweep scan. A Function generator outputs a voltage sweep which a Howland current source converts into an equivalent current sweep which is sent to the probe. Electrical properties of the probe are monitored via a Labview program as the probe is scanned across the surface of the test specimen.

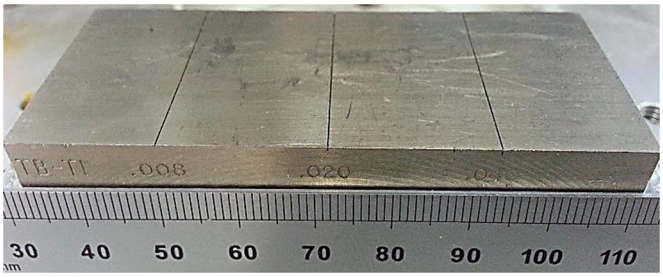

Fig. 8. Calibration block. Image of a Titanium 6Al – 4V test specimen and the three notches of increasing depth.

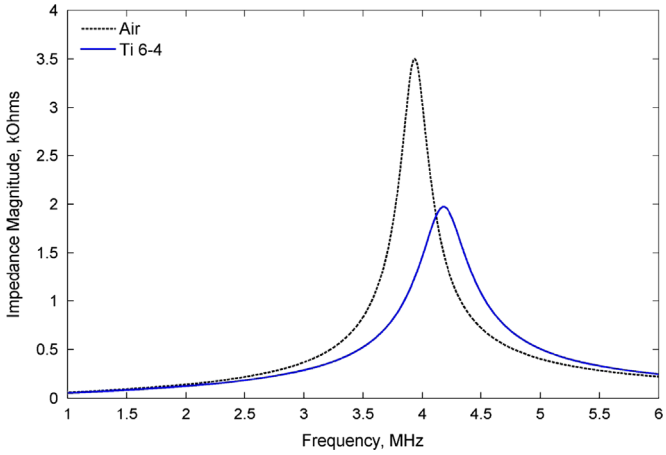

Fig. 9. Material coupling resonance shift. Impedance frequency profiles of the absolute probe in air and coupled to an undamaged section of a Ti 6-4 test specimen.

The effective resistance, or real component of the impedance of the system, now has frequency dependence, so it cannot be eliminated with traditional arguments. Instead the impedance must be fully expanded.

$$Z_1 = \frac{R_0 + \omega L_0(k^2/2) + j\omega L_0(1-(k^2/2))}{1 + j\omega C_0 R_0 + j\omega^2 C_0 L_0(k^2/2) - \omega^2 C_0 L_0(1-(k^2/2))}. \tag{10}$$

The general expression for the resonant frequency, ω_1, can be simplified for the specific case when the probe circuit has a large

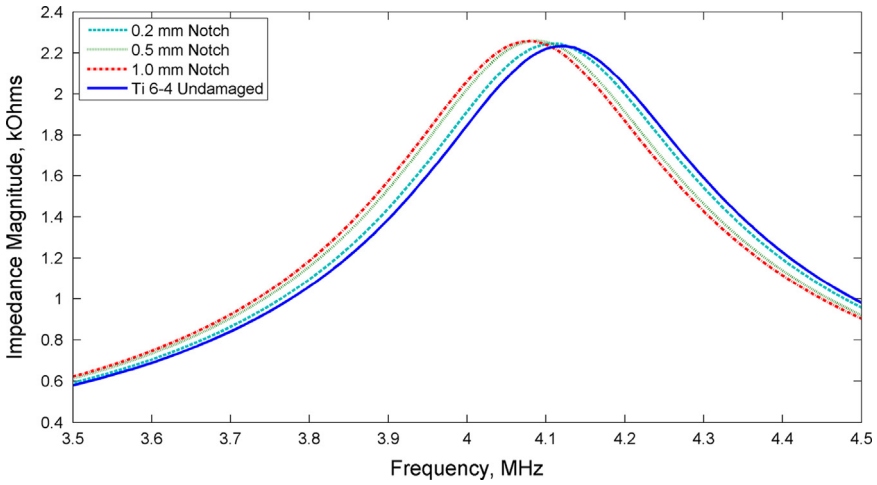

Fig. 10. Defect-decoupling resonance shifts in the presence of calibration slots. Impedance frequency profiles of the absolute probe on undamaged Ti 6-4 and above three notch defects of increasing depth.

Table 1
Resonant frequency of an ECT probe in air, above undamaged and three defects within Titanium 6-4 (zero liftoff).

Material	Defect	f_0 (± 0.003 MHz)	k (± 0.001)	L_1 (± 0.01 μH)
Air	–	3.938	0.000	10.34
Measurements under Kapton tape				
Ti 6–4	Undamaged (mm)	4.125	0.421	9.42
	0.20	4.113	0.408	9.48
	0.50	4.088	0.380	9.59
	1.00	4.075	0.364	9.65

quality factor [14] i.e. $R_0 \ll \omega L_0$,

$$\omega_1^2 = \frac{1}{C_0 L_0 \sqrt{1-k^2+(k^4/4)}} \equiv \frac{1}{C_0 L_0[1-(k^2/2)(1+j)]}. \tag{11}$$

Typical values for k are rarely greater than 0.5 for surface coupling in which case Eq. (11) can be approximated to,

$$\omega_1^2 \cong \frac{1}{C_0 L_0(1-(k^2/2))}. \tag{12}$$

The resonant frequency of the system is dependent on the coupling between the probe and the surface of the material [14]. An expression for the coupling coefficient can be derived from Eqs. (2) and (11) as a fuunction of the ratio between the resonant frequency of the probe in air, ω_0, and of the coupled system, ω_1.

$$k^2 \cong 2\left[1-\left(\frac{\omega_0}{\omega_1}\right)^2\right] \tag{13}$$

The coupling coefficient, k, is dependent on, and very sensitive to, many of the variables of the coupled system, i.e. conductivity, magnetic permeability, liftoff, material surface finish, tilt, frequency and temperature. As with any resonating system, even slight changes can have a large effect on the amplitude of oscillation. A change in k represents changes in the inductive and resistive components of the eddy-current circuit in Fig. 3. A reduction in the coupling coefficient, k, from that of the system coupled to the surface of an undamaged material will be referred to as decoupling. This could be due to an increase in liftoff from the sample (liftoff-decoupling) or the presence of a defect (defect-decoupling). Each will cause a shift in the resonant frequency of the system (resonance-shift).

An experimental investigation was carried out to investigate ECT operation at frequencies approaching electrical resonance and determine the effects, if any, of defect-decoupling resonance-shifts on ECT defect signals.

3. Experimental method

A single coil pen probe was used to investigate how operating at frequencies passing through resonance would affect the sensitivity of absolute ECT crack detection. The probe comprised 38 turns around a 1.02 mm ferrite core, within a ferrite cap (as shown in Fig. 6), and was connected to the source using a RG174 coaxial cable. The probe had a characteristic inductance in air of $L_0 = 10.34 \pm 0.09$ μH and the coaxial cable had a capacitance of $C_0 = 101$ pFm^{-1} [24].

The probe was operated in the absolute mode [3] and was driven by a current source sweeping through frequencies up to and beyond resonance in the MHz frequency range. In order to recreate industrial inspection conditions, all measurements with the probe were performed with a single layer of Kapton® tape between the coil and test material.

With reference to Fig. 7, a Tektronix 3021B arbitrary function generator was used to create a swept voltage input signal which was converted into an equivalent drive current within a Howland current source.

The Howland current source [25], built in house, converts voltages from the arbitrary function generator into a constant current, which is supplied to the load coil. As a result, the amplitude of the current through the coil never changes and is linearly proportional to the driving voltage amplitude, even as the coil enters different environments. Instead, the voltage across the coil (V_{out}) varies to maintain the constant current, and is thus the measured quantity within the scan. The properties of the Howland current source make it particularly useful in multi-coil probes, when passive measurements are made. The Howland source ensures that passive sensors will only measure changes in the eddy-current flow within the material, and not arbitrary changes in the current through the primary excitation coil.

The current source converts a sinusoidal ± 0.5 V signal into a sinusoidal ± 50 mA drive current, which is supplied to the probe via a 1.56 m length of RG174 coaxial cable. The voltage in (V_{in}),

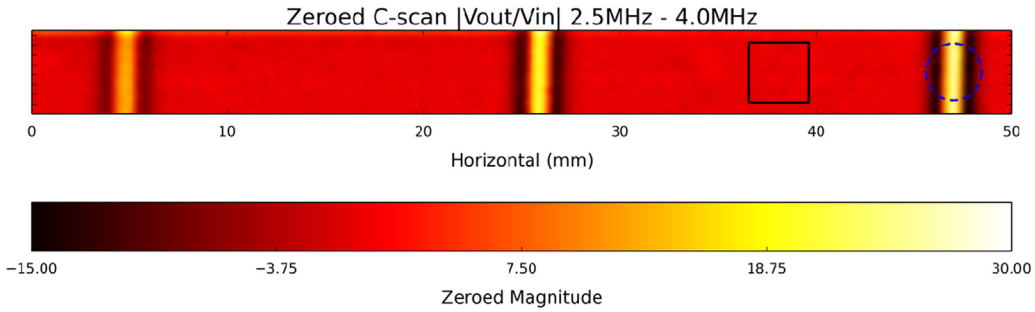

Fig. 11. Calibration block C-scan image. Frequency "collapsed" C-scan image of the material surface showing an example of where defect (blue dashed circle) and noise (black solid square) data is measured.

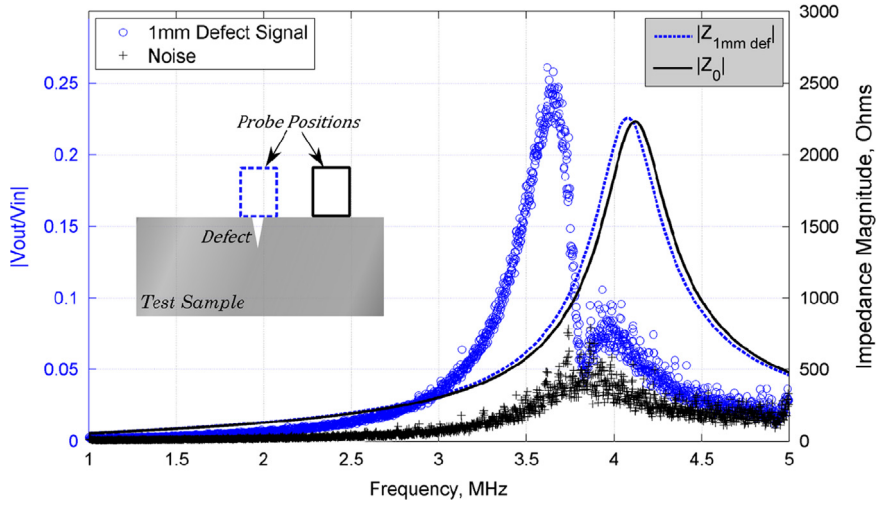

Fig. 12. Signal and noise. Defect signal (dashed blue) and rms noise (solid black) level for the 1.0 mm deep notch as a function of frequency. Also showing the associated resonant frequency shift of the probe in the presence of the defect. Probe locations on and off the defect are shown in a schematic diagram.

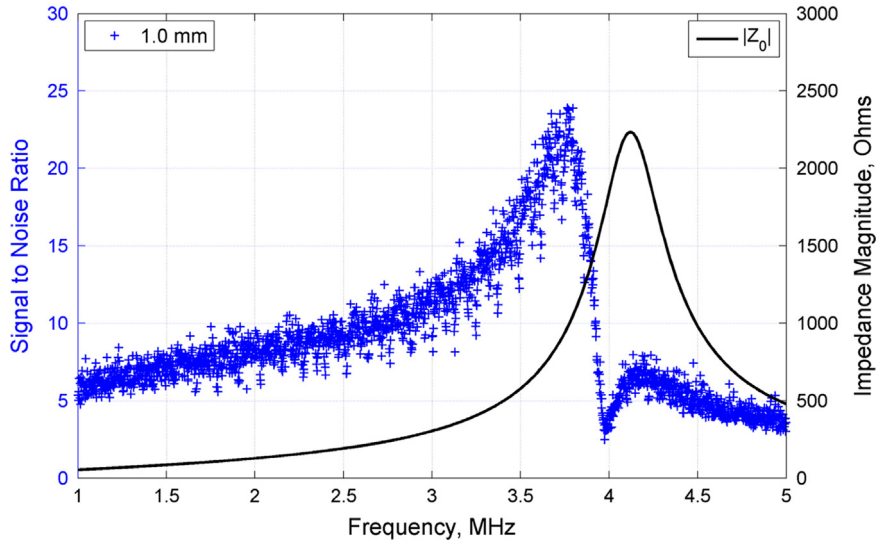

Fig. 13. Signal-to-Noise Ratio (SNR). Plot of the 1.0 mm defect as a function of frequency. The plot is shown in relation to the resonance peak of the impedance profile (solid black).

from the function generator, and the voltage across the probe (V_{out}), were monitored and recorded at a rate of 50 MSamples/s using a National Instruments Labview program (4), which also controlled the XY stage to scan the probe across the sample. For each step of the scan, V_{in} and V_{out} were recorded over one frequency sweep, and saved together in a binary file containing the probe co-ordinates. The ratio of V_{out} over V_{in} is proportional to the impedance, with the knowledge that $V_{in} = I_{in}R$.

Three large calibration notch defects in a Titanium 6Al–4 V (Ti 6-4) specimen (pictured in Fig. 8) were inspected, to investigate the effects of defect-decoupling resonance-shifts on defect signals. Ti 6–4 is one of the most widely used superalloys in the Aerospace

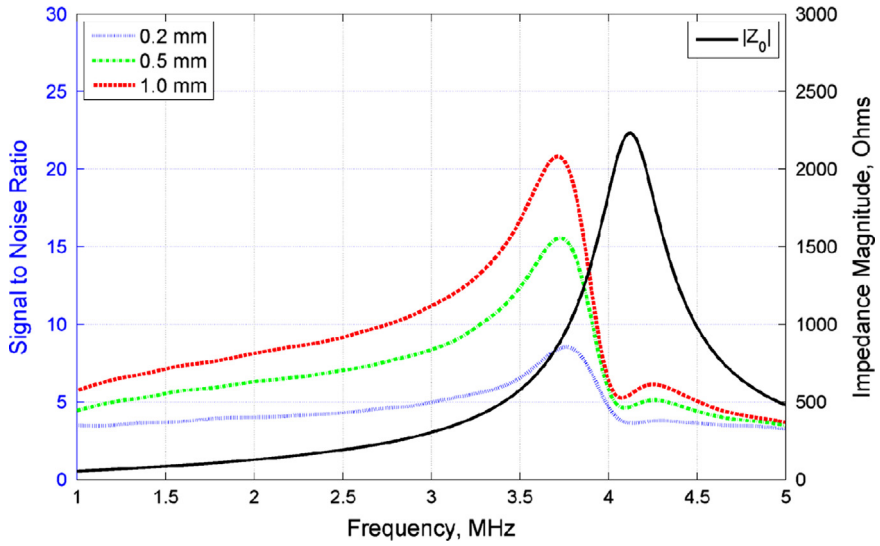

Fig. 14. Near electrical resonance signal enhancement. Experimental plot showing the SNR trends as a function of frequency for each defect. The plots are shown in relation to the resonance peak of the impedance profile (solid black).

Table 2
SNR peak details in experimental data for three defects of increasing depth with reference to SNR at 1 MHz.

Defect depth (mm)	SNR at 1 MHz	SNR Peak frequency ($\pm$0.01 MHz)	SNR at Peak	SNR Enhancement from 1 MHz
0.20	3.50	3.79	8.79	2.51
0.50	4.46	3.77	16.03	3.59
1.00	5.74	3.76	21.43	3.73

industry, and so is an ideal test specimen [1]. The notch defects spanned the width of the test sample, and had depths of 0.20, 0.50 and 1.00 mm (0.008, 0.020 and 0.040 in. respectively). Ti 6–4 typically has a conductivity of $\sigma_{Ti(6-4)} = 0.60 \times 10^6$ S m^{-1} and a relative magnetic permeability $\mu_{Ti\,(6-4)} = 1.00005$ [26].

A 4294A Agilent impedance analyzer was used to find the impedance of the eddy current probe and cable, as a function of frequency, $Z(f)$, of the probe in different environments. Fig. 9 shows the $Z(f)$ profiles of the probe both on (at zero liftoff with Kapton® layer), and off (in air) an undamaged section of the Ti 6–4 test piece. The $Z(f)$ profiles were also measured for the probe positioned directly above the three notch defects where the maximum frequency shift (defect-decoupling) occurred (Fig. 10).

The resonant frequencies, f_0, for each $Z(f)$ profile are shown in Table 1 along with the estimated coupling coefficient, k, calculated using Eq. (13), and the equivalent coil inductance, L_1, of the system, calculated using Eq. (8).

The resonant frequency shifts in Table 1 represent the defect-decoupling of the probe circuit with varying defect size. From the table, it is clear that the material condition affects the level of coupling that can be achieved by the system. It is these changes in the coupling, and therefore the resonant frequency, which give rise to a signal enhancing phenomenon.

4. Results

Three notches in the Ti 6–4 sample were tested using a single coil probe operated in the absolute mode and swept through frequencies from 1–5 MHz. A 0.52 ms repeating frequency sweep signal was generated using a 25 MSamples s^{-1} arbitrary function generator, to output a driver waveform that satisfies the Nyquist criterion.

The waveform was created to decrease exponentially with frequency (see Fig. 7) so that the V_{out} signal would not saturate the measurement scale as the frequency approached resonance. V_{in} and V_{out} were scaled such that their maxima, when coupled to undamaged Ti 6–4, were equal to 80% of full screen height. The resulting output signals, V_{in} and V_{out}, were converted into the frequency domain via Fourier Transform and 'binned' (bin width = 1923 Hz) over the full frequency range.

The ratio of V_{out} over V_{in} is proportional to the impedance of the system ($Z = V_{out}/I_{in}$). In this way a value proportional to the magnitude of the ECT defect signals, $|Z|$, was found for each position within the XY scan to build an image of the surface. The C-scan image was zeroed to an area of undamaged material. Fig. 11 shows a high contrast C-scan image of the test piece surface constructed by the linear combination of data from frequency bins within the frequency range of 2.5–4.0 MHz (avoiding resonance at 4.125 MHz).

At each frequency, the maximum signal strength magnitude, $S(f) = |V2/V1|$, of each defect and the root-mean squared (rms) noise level, $N_{rms}(f)$, of a 10×10 mm^2 area of undamaged material was recorded from the scan. The data was then plotted as a function of frequency (Fig. 12), and compared to the impedance magnitude profiles of the probe on the defect, and on an undamaged section of the material.

It is clear from Fig. 12 that there occurs a frequency, close to resonance, where the defect signal reaches a maximum. Note that the background noise reaches a peak at a higher frequency, where the defect signal reaches a local minimum. The resulting SNR plot as a function of frequency is shown in Fig. 13 for the 1.0 mm notch defect.

The broad distribution within the SNR plots could be a result of the background electronic noise produced by the XY scanning table. The SNR data was fitted with spline best fit curves (smoothing factor 0.99) to better display the shifting frequency of the signal peak with changing defect depth (Fig. 14). The exact frequencies of the SNR peaks are displayed in Table 2.

The SNR peaks occur in a region conventionally avoided by probe manufacturers and operators owing to the unpredictable and unstable nature of resonance. Conventional probe operating frequencies finish significantly short of the electrical resonance of the probe, keeping safely within a range where the sensitivity

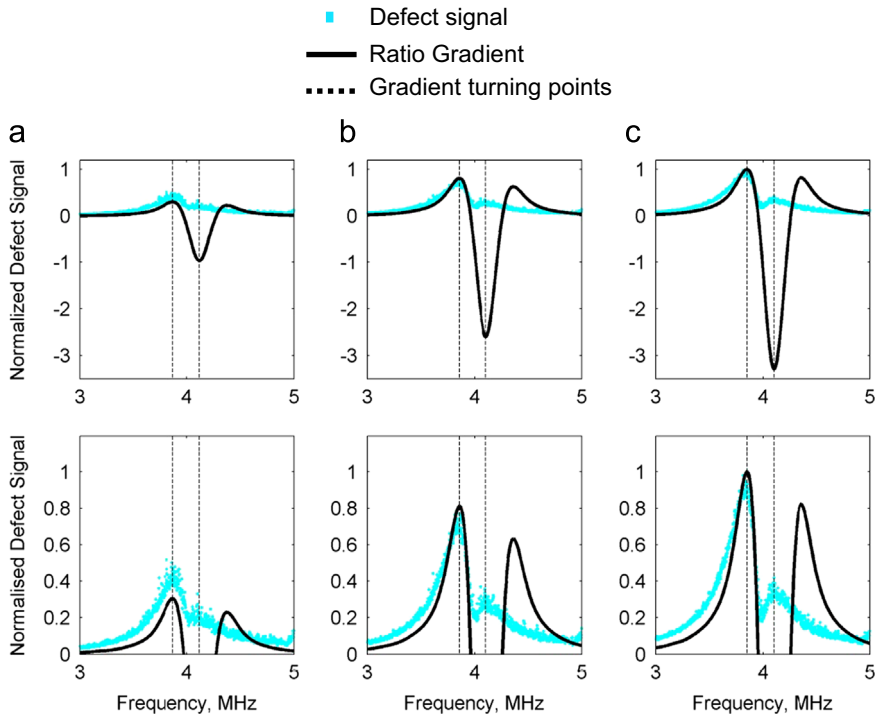

Fig. 15. Relationship between signal enhancement and defect-decoupling. Normalized 0.20 (a), 0.50 (b) & 1.00 (c) mm deep, defect signal strength compared, on the same scale, to the gradient of the ratio of defect-decoupled impedance. Plots are shown in full (top) and for positive signals (bottom). Dotted lines represent the frequencies of maxima and minima in the predicted gradient plot.

scales linearly with frequency due to the inductive reactance component of impedance (ωL).

Beyond resonance, the reactive component of the system is dominated by capacitive changes within the cable, such that successful measurements of the inductive changes are impossible so this region must be avoided. Between the conventional limit and the electrical resonance of the system lies a region of probe sensitivity dominated by the effects of defect-decoupling resonance-shifts, where significant SNR enhancement occurs. This has been termed the Near Electrical Resonance Signal Enhancement (NERSE) frequency band, or zone, and will be dependent on the probe, cable length, test material and defect size.

4.1. Finding the NERSE peak frequency (f_{NERSE})

The defect signal magnitude, $S(f)$, shown in Fig. 12, peaks as a result of resonance shifts caused by defect-decoupling of the probe as it passes over a defect. It occurs at a frequency where the difference in rate of change between the impedance on and off a defect is greatest. This can be expressed as the maximum gradient of the ratio between the defect-decoupled, $|Z_d(f)|$, and undamaged material-coupled, $|Z_1(f)|$, impedance profiles.

$$S(f) \propto \frac{d}{df}\left(\frac{|Z_d(f)|}{|Z_1(f)|}\right) \tag{14}$$

Using the impedance profile s of the three notch defects, Eq. (14) was calculated and compared to the defect signals, $S(f)$, for each defect. The scaled, predicted results are shown in Fig. 15, to make clear the direct relationship between Eq. (14) and the defect signals.

There is a strong correlation between peaks in the signal strength and the location of the maxima and minima of Eq. (14). Table 3 compares the predicted peak position of f_{NERSE} and the signal peak f_{NERSE} frequency, based on a spline best fit of the data, with a smoothing factor of 0.9998.

Table 3
Defect NERSE frequency peak positions based on experimental absolute ECT scan data and predicted from impedance profile data calculation.

Defect depth (mm)	Signal f_{NERSE} ($\pm$0.01 MHz)	Predicted f_{NERSE} ($\pm$**0.006 MHz**)
0.20	3.88	3.869
0.50	3.85	3.856
1.00	3.83	3.850

f_{NERSE} is dependent on the size of the defect, and will tend towards the frequency at which the gradient of $|Z_1(f)|$, the coupled impedance, is a maximum as the defect size decreases to zero. This sets an upper limit for the frequency of NERSE operation equivalent to the noise in resonance shifts on undamaged material. Beyond this frequency limit, the measurements of the electrical properties are complicated by high background noise and capacitive effects in the system.

There occurs a sharp minimum just before 4 MHz. This corresponds to the frequency where the rate of change of impedance tends towards a minimum as it reaches resonance. After resonance the system starts to become dominated by its capacitive components but the inductance will still have some effect. This is why there is a smaller secondary signal peak just beyond resonance.

5. Conclusions and future work

This paper has highlighted a band of frequencies, outside the conventional operation range, and close to electrical resonance of an eddy current probe, where the magnitude of impedance SNR reaches a peak. The SNR of scans of three slots of varying depth were enhanced by a factor of up to 3.7, from the SNR measured at 1 MHz. This is a result of a defect-decoupling resonance-shift effect and is referred to as the near electrical resonance signal enhancement (NERSE) phenomenon. NERSE frequency operation

has significant potential for ECT inspection, and opens up a range of investigative possibilities. Within this investigation, only the magnitude of the electrical impedance has been analyzed. An immediate extension of this investigation will be to consider phase information, and determine whether a similar exploitable NERSE effect exists.

In a break from conventional ECT, the identification of the NERSE frequency band has introduced the possibility of operating ECT probes at a single NERSE frequency (that of a target defect), in order to increase the probability of detecting smaller defects. Such an approach could improve the SNR for small defects where, at lower frequencies, the signal from the defect would be below the electrical background noise. This approach will also be investigated for detecting defects within materials of high levels of microstructural background noise. So long as the decoupling resonance-shift caused by the microstructure is less than that caused by any defects then a signal enhancement effect should be observed.

The electrical resonant frequency of an ECT system can be affected by a number of environmental factors including, but not limited to; temperature, liftoff, tilt and the degree of surface roughness. Operating at frequencies close to resonance will therefore lead to a greater sensitivity to these issues. However, for an automated inspection system, i.e. one controlled via robotic motion, serious liftoff and tilt variations can be suppressed such that resonance shifts from these factors are negligible compared to shifts resulting from the presence of defects. In all of the experiments carried out, no attempts to limit the effects of temperature were made. Variations in the temperature and surface roughness can be filtered out using a band-pass filter. So long as these factors do not vary in the extreme, so that the level and spatial distribution of resonance shifting they produce is comparable to that of defect shifts, the SNR improvement will still be observed. These factors become more of an issue the smaller the target defect becomes. Future work will investigate the limits of this.

In addition to the use of NERSE frequencies in single coil inspections stated above, there are other promising applications for the additional information sweeping through resonance offers. Sizing and profiling may be possible, by carefully locating the peak frequency of swept defect signals, and ascertaining the level of defect-decoupling associated with a given defect in order to determine its approximate or relative size. Finally, the complex resonance interactions that occur in densely populated eddy-current arrays (ECAs) will be examined. The focus will be on exploiting the NERSE phenomenon in transmit-receive and arrayed probes in order to achieve greater sensitivity.

The prospect of improving sensitivity through a simple procedural change, without the need for complex probe design or data analysis, is a potentially valuable complementary technique to any ECT method.

Acknowledgments

Many thanks go to Rolls-Royce plc. and the Research Centre for Non-Destructive Evaluation (RCNDE) for their support, funding and encouragement. Credit also goes to Rolls-Royce NDE lab, Bristol UK, for the use of the X-Ray CT system.

References

[1] Boyer RR. Titanium for aerospace: rationale and applications. Adv Perform Mater 1995;2(4):349–68.
[2] Gros XE, Bousigue J, Takahashi K. NDT data fusion at pixel level. NDT E Int 1999;32(5):283–92.
[3] García-Martín J, Gómez-Gil J, Vázquez-Sánchez E. Non-destructive techniques based on Eddy current testing. Sensors 2011;11(3):2525–65.
[4] Abu-Nabah B, Hassan W, Ryan D, Blodgett M, Nagy P. The effect of hardness on Eddy current residual stress profiling in shot-peened nickel alloys. J. Nondestruct. Eval. 2010;29(3):143–53.
[5] Blodgett MP, Nagy PB. Eddy current assessment of near-surface residual stress in shot-peened nickel-base superalloys. J. Nondestruct. Eval. 2004;23 (3):107–23.
[6] Grimberg R, Udpa L, Savin A, Steigmann R, Palihovici V, Udpa SS. 2D Eddy current sensor array. NDT E Int 2006;39(4):264–71.
[7] Huang H, Sakurai N, Takagi T, Uchimoto T. Design of an eddy-current array probe for crack sizing in steam generator tubes. NDT E Int 2003;36(7):515–22.
[8] Zilberstein V, Walrath K, Grundy D, Schlicker D, Goldfine N, Abramovici E, et al. MWM eddy-current arrays for crack initiation and growth monitoring. Int J Fatigue 2003;25(9–11):1147–55.
[9] Bartels KA, Fisher JL. Multifrequency eddy current image processing techniques for nondestructive evaluation. In: Proceedingsof the International Conference onImage Processing; 1995.
[10] Liu Z, Tsukada K, Hanasaki K, Ho YK, Dai YP. Image fusion by using steerable pyramid. Pattern Recogn Lett 2001;22(9):929–39.
[11] Chady T, Sikora R. Optimization of eddy-current sensor for multifrequency systems. IEEE Trans. Magn. 2003;39(3):1313–6.
[12] Liu Z, Tsukada K, Hanasaki K, Kurisu M. Two-dimensional Eddy current signal enhancement via multifrequency data fusion. Res Nondestruct Eval 1999;11 (3):165–77.
[13] Zheng L, Forsyth DS, Komorowski JP, Hanasaki K, Kirubarajan T. Survey: state of the art in NDE data fusion techniques. Instrum Meas IEEE Trans 2007;56 (6):2435–51.
[14] Owston CN. A high frequency eddy-current, non-destructive testing apparatus with automatic probe positioning suitable for scanning applications. J Phys E Sci Instrum 1970;3(10):814.
[15] Liu C, Dong Y. Resonant enhancement of a passive coil-capacitance loop in eddy current sensing path. Measurement 2012;45(3):622–6.
[16] Liu CY, Dong YG. Resonant coupling of a passive inductance-capacitance-resistor loop in coil-based sensing systems. IEEE Sens J 2012;12(12):3417–23.
[17] Ko RT, Blodgett MP, Sathish S., Boehnlein TR. Resonant Frequency Eddy Current Liftoff Measurements for Shot Peening Intensity Assessment in Materials, DTIC Document; 2007, (Preprint).
[18] Ko RT, Blodgett MP, Sathish S, Boehnlein TR. Application of resonant frequency eddy current technique on a shot-peened nickel-based engine-grade material. In: Thompson DO, Chimenti DE. editors. Review of Progress in Quantitative Nondestructive Evaluation. Vol nos. 26A and 26B, American Institute of Physics: Melville; 2007. p. 1608–15.
[19] Blitz J. Electrical and magnetic methods of non-destructive testing. London: Chapman & Hall; 1997.
[20] Horowitz P, Hill W. The art of electronics. Cambridge: Cambridge University Press; 1989; 1152.
[21] White JF. High frequency techniques: an introduction to rf and microwave engineering. New Jersey: Wiley; 2004.
[22] Wheeler HA. Formulas for the skin effect. Proc IRE 1942;30(9):412–24.
[23] Bleaney BI, Bleaney B. Electricity and magnetism. Oxford: Oxford University Press; 1989.
[24] RS Online. 13/08/13; Available from: ⟨http://uk.rs-online.com/web/p/coaxial-cable/5218206/⟩.
[25] Anudev, J. and Raglend, I.J. Analytical study of howland current source model. In: International Conference on. Computing. Electronics and Electrical Technologies (ICCEET); 2012.
[26] Welsch G, Boyer RF, Collings EW. Materials properties handbook: titanium alloys. Ohio, USA: ASME International; 1994.